

# HARD X-RAY AND MICROWAVE FLUX SPECTRA OF THE 2 NOVEMBER 1991 SOLAR FLARE

CHIK-YIN LEE<sup>1,2</sup> and HAIMIN WANG<sup>1</sup>

<sup>1</sup>*Big Bear Solar Observatory, New Jersey Institute of Technology, 40386 North Shore Lane,  
Big Bear City, CA 92314-9672, U.S.A.*

<sup>2</sup>*Department of Physics, Rutgers University, Newark, NJ 07102-1811, U.S.A.;*  
*e-mail: chikyin@solar.njit.edu*

(Received 24 August 1998; accepted 5 March 2000)

**Abstract.** We analysed the hard X-ray and microwave flux spectra of the solar flare (BATSE No. 1791) on 2 November 1991, which started at 16:11:03 UT and ended at 16:56:10 UT. This flare is particularly interesting because of its deep cyclic intensity modulation. Data are available simultaneously from the 16-channel BATSE/LAD hard X-ray and 45-frequency OVRO microwave database. We quantitatively compare the time variations in profiles of the hard X-ray spectral photon index, the 50 keV X-ray flux, and microwave spectral indices (at both high and low frequency ends). As expected, the X-ray photon spectral index decreases as the hard X-ray flux increases. This pattern appears in all the sub-peaks. This is consistent with previous observations that hard X-ray emission hardens at the emission peak. However, the behaviour of the high-frequency microwave index is unexpected. We observe an anti-correlation between the high-frequency microwave index and the hard X-ray photon index during the course of the flare. Finally, we study the arrival time of microwave flux peaks as a function of frequency and find that the microwave peak at a higher frequency comes earlier than that at a lower frequency. A maximum delay of 72 s is found among the main peaks at different frequencies. Shorter delays are found for the other five sub-peaks.

## 1. Introduction

The electrons which produce hard X-ray emissions in solar flares have long been considered to come from the same population that are responsible for microwave bursts (Dennis, 1988). Particularly well studied is the comparison of the time profiles. It is well known that the temporal variation of impulsive microwave and hard X-ray flux profiles during flares are remarkably similar (Dennis and Schwartz, 1989; Kai *et al.*, 1983), except that the impulsive microwave bursts tend to peak a few seconds later and fall more slowly (Crannell *et al.*, 1978; Cornell *et al.*, 1984; Kaufmann *et al.*, 1983; Lu and Petrosian, 1990). Some VLA observations with arc second spatial resolution, however, show that the microwaves and hard X-rays are not co-spatial (see review by Dulk, McLean, and Nelson, 1985, and references therein). In one of the earlier studies that used both radio and hard X-ray spectral data, Marsh and Hurford (1980) concluded that the electron populations that respectively produced microwave and hard X-ray emissions are spatially and spectrally separated, despite a temporal similarity between the flux profiles.



Comparisons of evolutionary properties of hard X-ray spectra and microwave spectra should provide more comprehensive information on the relationship between the electrons producing these two kinds of emissions. For example, the evolution of hard X-ray photon index should correlate with that of the microwave high-frequency spectral index if the same group of electrons is responsible for both emissions. Such a study has never been done. A combination of microwave data from OVRO and hard X-ray data from BATSE provides an excellent opportunity for this study.

This paper studies the hard X-ray and microwave spectra of the solar flare on 2 November 1991. The existence of a total of six distinguishable peaks in both microwave and X-ray flux profiles makes this solar flare particularly interesting. A closer look at the flux profiles reveals that four sub-peaks can be identified before the main peak. In this study the microwave data were obtained by the solar array at the Owens Valley Radio Observatory (OVRO), while the hard X-ray data are available from the Compton Gamma Ray Observatory/Burst and Transient Source Experiment/Large Array Detector (CGRO/BATSE/LAD) database.

Hard X-rays and microwaves are generated by different physical processes, namely bremsstrahlung and gyro-synchrotron radiation. Observing parameters, such as the hard X-ray photon index, microwave low and high frequency slopes, and microwave peak frequency (see below), are defined based on these radiation models. The time evolution of these parameters during the flare is compared. The presence of the sub-peaks contains richer information for the correlation study of time profiles than single peak flares.

It is often observed that microwaves peak later than hard X-rays. A model of electron acceleration plus trapping proposed by Gary and Tang (1985) tried to account for the delay. The energy dependence of the time delay in hard X-rays and the frequency dependence of the time delay in microwaves were studied by Takakura *et al.* (1983) using five microwave frequencies. A long time delay between peaks of intense hard X-rays and microwaves in the range from 5 to 10 s was reported. We further study the time delay by using many more frequencies in the analysis for the present flare. The microwave time delays of all the individual sub-peaks are included in our analysis.

In this paper, the study of the 2 November 1991 solar flare is divided into two parts. Firstly, we will define several observing parameters and compare their time profiles. Secondly, we investigate the frequency dependence of the delay time in microwaves, and also the energy dependence of the delay time in hard X-rays.

## 2. Observations

This major flare (M4.8) was observed by the OVRO solar array and CGRO/BATSE/LAD on 2 November 1991. The five antennas of the OVRO solar array were arranged in a ‘T’ configuration with two 27-m antennas located on the east arm

at 61 m and 488 m east of the centre pad; one 2-m antenna on the west arm at 183 m west of the centre pad; and two 2-m antennas on the north arm at 122 m and 366 m north of the centre pad. The array was operated with an observing sequence that sampled 45 frequencies in the range of 1-18 GHz every 12 s in both right-hand circular polarization (RCP) and left-hand circular polarization (LCP). The amplitude and phase of each baseline were calibrated relative to the bright radio nuclei of NGC1275 (3C 84) every two hours. In this paper, we primarily use the flux measurements of the two 27-m antennas.

The BATSE observations of solar flares were described in detail by Schwartz *et al.* (1993). BATSE has both Large Area Detectors (LAD, over 2000 cm<sup>2</sup> per detector) and spectroscopy detectors (SD, 127 cm<sup>2</sup> per detector) to improve sensitivity, time resolution, and spectral resolution. This paper uses the 16-channel LAD/CONT data and also the 6-channel LAD/DISCLA data.

### 3. Correlation Study Among Various Time Profiles

#### 3.1. DEFINITIONS OF OBSERVING PARAMETERS

During a solar flare, fast electrons emit radiation while moving inside a magnetic loop after magnetic reconnection has taken place. The mechanism that produces hard X-rays is called bremsstrahlung radiation. This free-free radiation is produced by electrons, which are stopped on reaching the chromospheric foot-points. On the other hand, microwaves with frequency of the order of 10 GHz are produced by gyro-synchrotron radiation. It is believed that the microwave radiation is emitted by the same population of electrons that produce hard X-rays. Some of the radio producing electrons may be trapped within the flux loop and bounce back and forth until they lose all their kinetic energy.

We make use of the symbol  $F_{\text{HXR}}(t, E)$  to denote the hard X-ray flux spectrum, which is a function of time  $t$  and photon energy  $E$ . For the microwave flux, the corresponding spectrum is expressed as  $F_m(t, f)$ , where  $f$  is the microwave frequency. Figures 1(a) and 1(b) show the spectral profiles of  $F_{\text{HXR}}(E)$  and  $F_m(f)$  around the main peak of the flare at 16:34:53 UT. They are functions of energy (hard X-ray) and frequency (microwave) respectively. On the other hand, Figures 2(a) and 2(b) show the hard X-ray and microwave time profiles of  $F_{\text{HXR}}(t)$  and  $F_m(t)$  at 50 keV photon energy and 5.0 GHz microwave frequency, respectively.

Assuming an initial injection of non-thermal electrons with a power-law energy distribution, it is possible to calculate and express the radiation flux in an explicit form by using the Bethe–Heitler cross section. The resulting photon flux is also given by a power law,

$$F_{\text{HXR}}(E) = CE^{-\gamma} \quad (\text{counts s}^{-1} \text{ cm}^{-2} \text{ keV}^{-1}),$$

where  $E = h\nu$ . The straight line in Figure 1(a) represents the result of such a fitting by  $F_{\text{HXR}}(E) = CE^{-\gamma}$ . The X-ray photon index, also known as spectral index, is

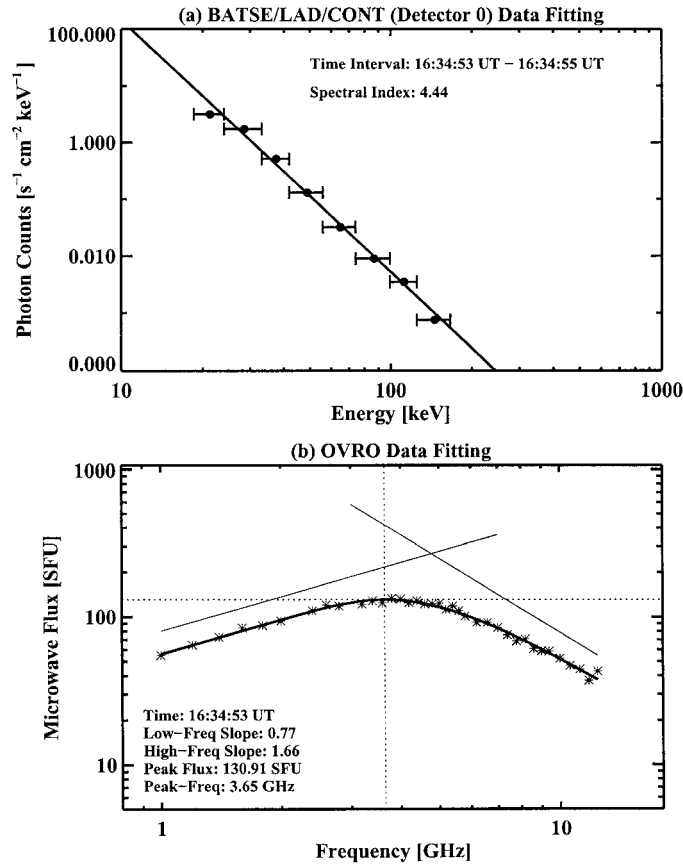


Figure 1. (a) BATSE/LAD/CONT X-ray data fitting. The X-ray flux is assumed to be a simple power law in energy. The X-ray flux is assumed to be a simple power law in energy. Data are represented by short horizontal error bars. The spectral index is defined as the negative of the slope of the straight line in the log-log scale plot. (b) OVRO microwave data fitting. In order to have a better least-square curve fitting, only the first 37 frequencies, from 1.0 GHz to 12.4 GHz, are considered. The displayed flux curve represents one of these fittings. The horizontal and vertical dotted lines locate the peak flux and peak frequency respectively. The two tilted straight lines define slopes at low and high frequencies. The dotted vertical line also divides regions into optically thick and thin part.

defined as  $\gamma$ . It is equal to the negative of the slope of the straight line found by least-square fitting of the data points.

Other physical parameters will be derived from the microwave data. We can define low and high frequency slopes, peak frequency, as well as peak flux graphically. In Figure 1(b), for example, the microwave flux curve peaks at 3.65 GHz, and then declines at higher frequencies because the radiation becomes optically thin at these frequencies. The transition frequency is thus known as the peak frequency. The slope of the straight line, found by fitting of the optically thick part of the flux curve at low frequencies, is defined as the low-frequency slope. Similarly, the

high-frequency slope is obtained by a linear fitting of the optically thin part of the flux curve at higher frequencies.

Generally, we can fit the flux profile  $F_m(f)$  as a function of frequency  $f$  at a given time  $t$  to the following formula (Stahli, Gary, and Hurford, 1989):

$$F_m(f) = Af^a[1 - \exp(-Bf^{-b})] \quad (\text{s.f.u.}) .$$

Mathematically, it can be shown that

$$\frac{\partial \ln F_m}{\partial \ln f} = a + \frac{\xi}{1 - \xi} ,$$

where  $\xi$  is given by

$$\xi = \frac{\exp(-Bf^{-b})}{1 - \exp(-Bf^{-b})} .$$

We have in the low-frequency limit

$$\left( \frac{\partial \ln F_m}{\partial \ln f} \right)_{f \rightarrow 0} = a ,$$

and in the high-frequency limit

$$\left( \frac{\partial \ln F_m}{\partial \ln f} \right)_{f \rightarrow \infty} = a - b .$$

Once the four variables in the formula are found by fitting, the low and high-frequency slopes are given by  $a$  and  $b - a$ , respectively. They are sometimes known as microwave spectral indices. The peak frequency and peak flux are then obtained by numerical interpolation.

The last parameter that we will discuss is the phase difference observed on the OVRO interferometer baseline that is formed by the two 27-m antennas. The phase difference provides relative positional information about the emitting source in the direction along the baseline. The importance of all parameters defined so far will be explained in the following subsections. The temporal variations of these parameters are plotted as functions of time in Figure 2. The key component of this section is the correlation study of the aforementioned parameters derived from the hard X-ray and microwave spectra.

### 3.2. MICROWAVE AND X-RAY FLUX PROFILES

$F_{\text{HXR}}(t)$  and  $F_m(t)$  represent the flux profiles at a specific X-ray photon energy and a microwave frequency respectively. Let us start with the comparison between the flux profile of hard X-rays at 50 keV with that of microwaves at 5.0 GHz. They are shown in Figures 2(a) and 2(b), respectively. The two profiles look quite similar in appearance. Four sub-peaks before the main peak and one sub-peak after the main

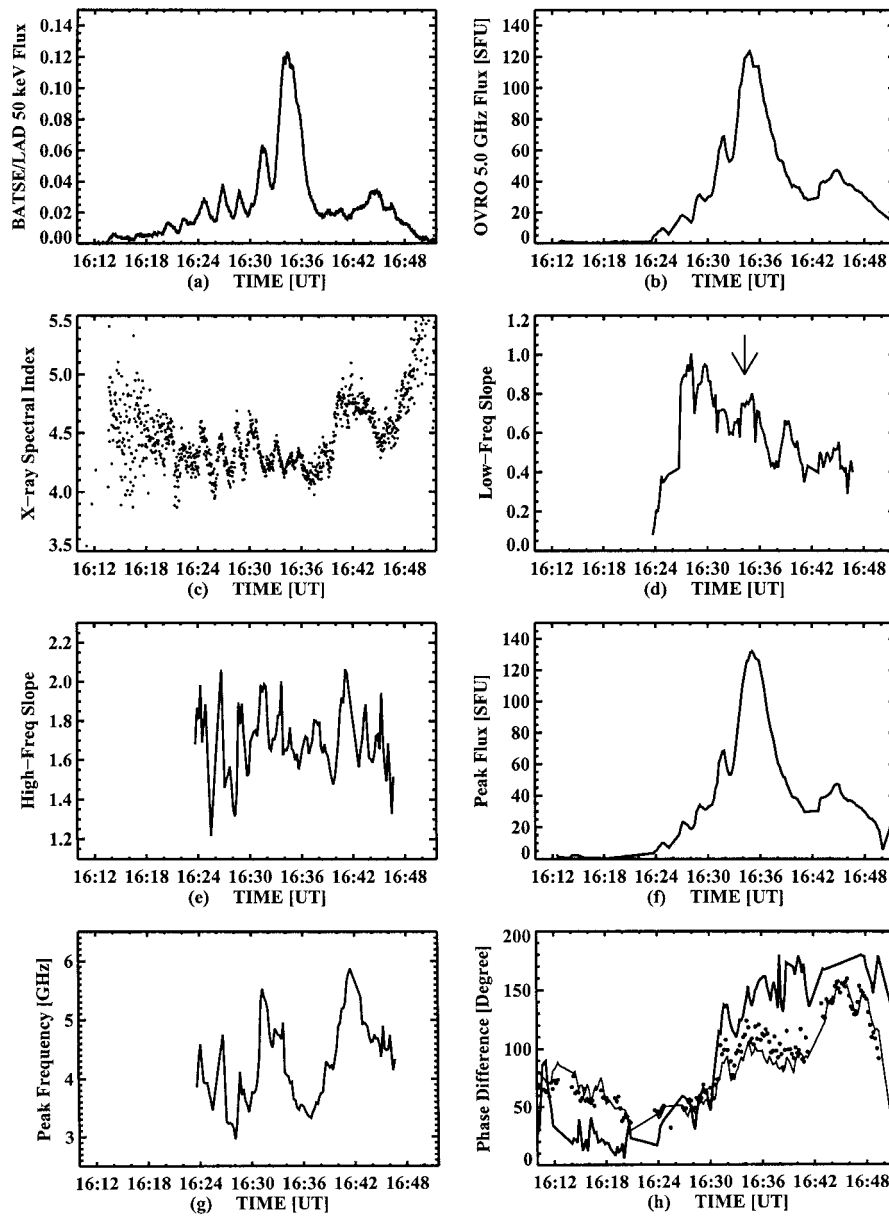


Figure 2. Various time profiles for the correlation study. The temporal resolution is 2 s for X-rays and 12 s for microwaves. The first two profiles are (a) X-ray flux at 50 keV and (b) microwave flux at 5.0 GHz. Profiles of derived physical parameters are shown in (c), (d), (e), (f), and (g). The observed relative phase evolution of two 27-m antennas is given in (h).

peak can be identified and matched in both the profiles. The smaller amplitude of modulation in the microwave profile may be due to low temporal resolution, and also indicates evidence of electron trapping in the microwave profile. There are temporal shifts of microwave peaks relative to X-ray peaks. Similar temporal shift is observed at other microwave frequencies. We will explore this point further in the following sections. It is important to point out that all the microwave flux profiles  $F_m(t)$  at different frequencies are well correlated to one another: an increase in flux at one frequency would imply an increase in flux at all other frequencies.

### 3.3. X-RAY SPECTRAL INDEX

The equation  $F_{\text{HXR}}(t, E) = CE^{-\gamma}$  implies that the X-ray flux  $F_{\text{HXR}}(t)$  has a functional dependence on the spectral index  $\gamma(t)$  since the dependent variable  $C(\gamma)$  is also a function of  $\gamma$  (and other physical parameters too). The spectral index is higher than 3.5 as indicated in Figure 2(c). The existence of sub-peaks should enable us to identify any relationship between the two profiles easily.

Figure 3(a) compares time profiles of the 50 keV X-ray flux and the X-ray photon index. It is shown that the two profiles gradually change from a positive correlation to a negative correlation across the main peak. At the vicinity of the main peak the X-ray global flux maximum can be matched to a corresponding local spectral index minimum. This anti-correlation has been observed by many earlier studies. However, it is interesting to find a positive correlation between the profiles for the three earliest peaks. After the main peak, the spectral index demonstrates the so-called soft-hard-soft pattern in the figure, which is a result of the fact that emissions are harder at flux peaks.

### 3.4. MICROWAVE LOW-FREQUENCY SLOPE

We begin the discussion with the source function which is defined as the ratio of emissivity to absorption coefficient. At low frequencies the emitting medium becomes optically thick and the radiation flux is proportional to the source function. The frequency dependence of the source function can be written as  $\nu^\alpha$ . Assuming a fixed source size, it can be shown that  $\alpha = 2.0$  for gyro-synchrotron emission (Gary and Hurford, 1989) with a thermal source in which the initial velocity distribution of electrons is Maxwellian, and a log-log plot of flux versus frequency would yield a low-frequency slope of 2.0. On the other hand, for a frequency-independent source size,  $\alpha$  will be 2.9 for a purely non-thermal gyro-synchrotron emission in which the distribution of injected electrons is a power law in energy.

It is clear from Figure 2(d) that the low-frequency slope is always less than 1.2. One would expect a value for the slope to be somewhere between 2.0 to 2.9 since a non-thermal source tends to increase the low-frequency slope by 0.9 (from 2.0 to 2.9, Dulk, 1985) for gyro-synchrotron emission. The result indicates that the source size decreases with increasing frequency. For example, if the solid angle of a flare

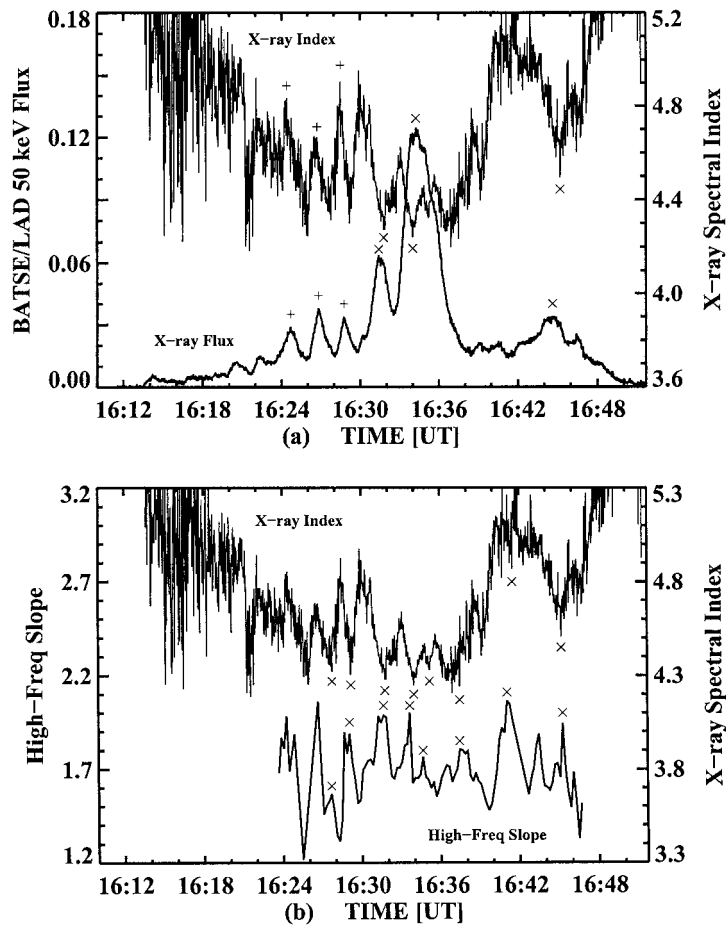


Figure 3. A detail correlation study on selected profiles. The markings '+' and 'x' represent positive and negative correlations respectively. (a) Profiles of X-ray spectral index and hard X-ray 50 keV flux. The first three flux peaks are positively correlated with the spectral index, while the last three flux peaks are negatively correlated with the spectral index. (b) Profiles of high-frequency slope and X-ray spectral index. A major anti-correlation between the two profiles is observed during the flare.

source is proportional to  $\nu^{-\eta}$ , then the low-frequency slope would be lowered by a factor of  $\eta$  (Bastian and Gary, 1992).

The additional information given by Figure 2(d) is a general decrease in the index of low-frequency slope with time. As thermal bremsstrahlung from the soft X-ray plasma becomes important, especially at low frequencies, it may help to flatten the radio spectrum when the contribution from gyro-synchrotron radiation begins to diminish. In order to investigate such possibility, we make use of the GOES soft X-ray flux to make comparisons since the microwave free-free emission should look a lot like the GOES profile. The plots are shown in Figure 4. The GOES flux continues to increase throughout the flare, and the microwave optically

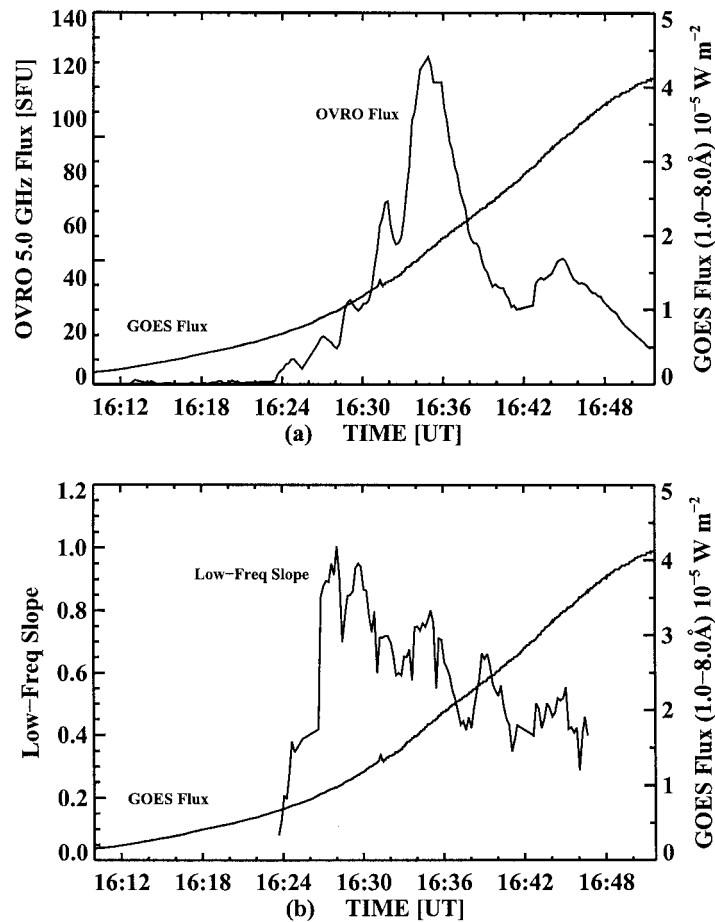


Figure 4. Plots of GOES soft X-ray flux in comparison with (a) microwave flux at 5.0 GHz and (b) microwave low-frequency slope. Note that GOES flux increases during the decreasing phase of the microwave flux and the low-frequency slope profile.

thick index decreases in response. As far as the thermal property is concerned, the observation could be interpreted in terms of a stronger thermal component due to microwave free-free emission presented at the later stage of the flare. However, this explanation is not strong: the microwave flux does not follow soft X-ray flux closely. So it is hard to be convinced that this thermal component gets into microwave spectra. If there is any thermal contribution, that is probably in a different component, such as super-hot component (Schwartz *et al.*, 1993).

### 3.5. MICROWAVE HIGH-FREQUENCY SLOPE

At high frequencies, the microwave-radiating source becomes optically thin. The microwave flux decreases as the frequency increases. The flux is proportional to the

emissivity which has a frequency dependence that goes as  $\nu^{-\beta}$ , where  $\beta$  is a positive number. For thermal gyro-synchrotron emission, the flux falls off very rapidly above some frequencies. However, a value between 1.5 to 4.2 is expected for a non-thermal gyro-synchrotron radiation (Dulk, 1985), and it is linearly proportional to the power index  $\delta$  of the non-thermal injection electrons. Under the assumption of a thick-target model, the hard X-ray photon index is given by  $\gamma = \delta - 1.5$ , and the high-frequency microwave index is given by  $\beta = 0.90\gamma + 0.13$ . From Figure 2(e) the index is found to be between 1.2 and 2.2. It should be noticed that the value of  $\beta$  deduced from  $\gamma$  does not indicate a steep fall off of flux as well, we therefore conclude that the flare is non-thermal in nature, especially near the peak of the flare. In many studies, the hard X-ray spectral index and the optically thin radio spectral index are incompatible (Nitta *et al.*, 1991; Melnikov and Magun, 1998; Silva, Wang, and Gary, 1999). In our case,  $\gamma = 4.2$ , this implies  $\beta = 3.9$ , whereas  $\beta = 1.7$  is observed. The discrepancy between the two indices is considered to be rather large.

A rather surprising result is obtained by a comparison between Figures 2(c) and 2(e), which is repeated in more detail in Figure 3(b). The local maxima of the high-frequency slope and the corresponding X-ray photon index minima are marked by ‘x’ in Figure 3(b). If microwave and hard X-ray emissions indeed originate from the same group of electrons, the microwave high-frequency slope should be linearly proportional to the hard X-ray photon index, and we would expect a positive correlation between the two profiles. The illustration in Figure 3(b), on the contrary, clearly indicates a major anti-correlation between the hard X-ray photon index and the microwave high frequency slope during the flare. We will attempt to explain this abnormality in term of the ‘trap-plus-precipitation’ model in the conclusion part.

### 3.6. MICROWAVE PEAK FREQUENCY AND FLUX

The maximum value of the flux curve  $F_m(f)$  is called the peak flux. It is the flux emitted at a peak frequency where the optical depth is of the order of unity. The flux begins to decline thereafter as the frequency continues to increase. One can easily identify the correlation between the microwave flux at 5.0 GHz and the peak flux in Figures 2(b) and 2(f).

The peak frequency, also known as turnover frequency, is the frequency at which the radiating source changes from optically thick to optically thin. From Figure 2(g) the peak frequency is found to be between 3.0 and 6.0 GHz. Physically, the peak frequency would increase when the emission comes from region of stronger magnetic field or higher column density. Comparing Figures 2(g) and 2(b), we do not observe any obvious correlation between the peak frequency and microwave flux.

### 3.7. PHASE VARIATION PROFILE

Having discussed the physical parameters derived from observational data, let us look at the phase signals recorded directly by the OVRO's two-element interferometer. If we assume a homogeneous emitting source with a constant size, any temporal change of phase difference detected by the east-west oriented interferometer would indicate a displacement of the source in the same direction. The phase profile as a function of time, therefore, contains spatial information for the solar flare.

Figure 2(h) shows three of the phase difference profiles. The thin and dotted lines represent phase profiles recorded with RCP at 5.0 GHz and 10.6 GHz, respectively. The profile represented by the thick line is recorded with LCP at 5.0 GHz. All the phase profiles are expected to be correlated if the interferometer is indeed observing a moving source. A clear correlation does exist between the two 5.0 GHz phase profiles of left-hand and right-hand circular polarizations. A similar positive correlation is also observed for the 10.6 GHz profile. This phase study therefore suggests the presence of a non-stationary emitting source. For example, a change in phase difference of 63 deg at 5.0 GHz between 16:34:51 UT and 16:44:51 UT was recorded, reflecting a relative shift in the source position of 5 arc sec in the EW-direction. An average velocity of  $14.8 \text{ km s}^{-1}$  is estimated for the source movement between 16:39:39 UT and 16:44:51 UT in the same direction. This gives a lower limit for the velocity because of the projection effect.

## 4. Frequency and Energy Dependence Study of Peak Time

### 4.1. FREQUENCY DEPENDENCE OF MICROWAVE PEAK TIME

We have already discussed the microwave flux profile at 5.0 GHz in the correlation study, and we are now going to consider other frequencies. It will be shown that the peak time is frequency dependent. This is one of the most important results of our study. But, first of all, let us define the peak time.

From a given microwave flux time profile, the flux maximum  $F_m^p(t_p, f)$  for a localized peak is easily located and the corresponding universal time is recorded. The superscript  $p$  is introduced here in order to distinguish which peak we are looking at. The universal time  $t_p$  is defined as the peak time for a specific peak under consideration, where  $p = 1, 2, 3, 4, 5$ , and 6. The main peak and the first peak are denoted by  $p = 5$  and  $p = 1$ , respectively.

The results are summarized by plotting peak time  $t_p(f)$  as a function of frequency. We try to use all 45 frequencies. However, we have to ignore some frequencies because the signal to noise ratio is too low and it is impossible to locate peaks at these frequencies. The excluded frequencies are either at the high or low end of the microwave spectrum. Six plots are shown in Figure 5. The temporal resolution is improved to 6 s as the data are combined from both 27-m antennas.

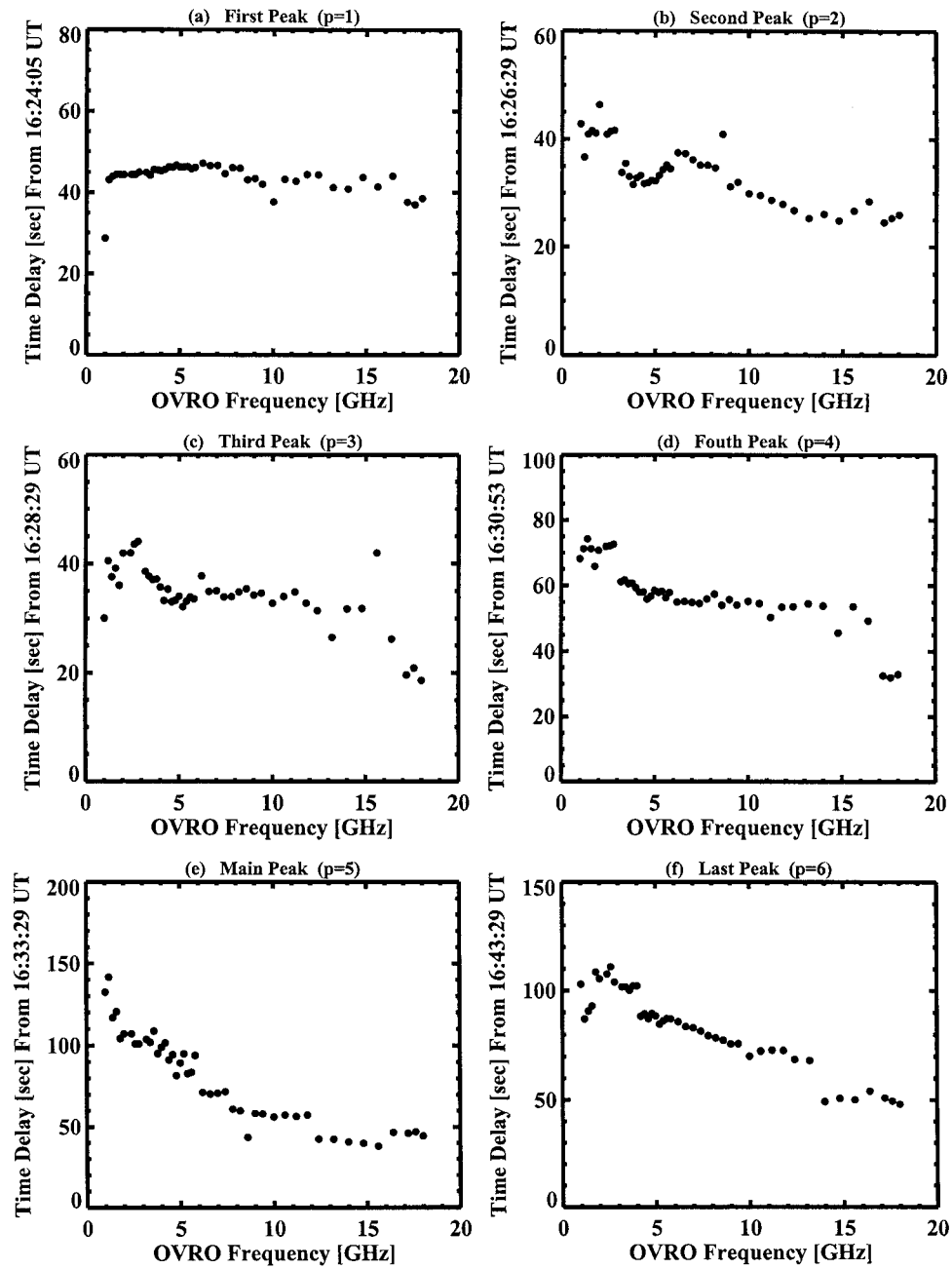


Figure 5. The peak time as a function of microwave frequency for each individual peak is shown. It can be seen that the peak time decreases as the frequency increases in all six plots. The data points actually represent averaged peak times recorded from the two different antennas.

From the plots in Figure 5, we come to the conclusion that the peak time is a generally decreasing function of microwave frequency. Among the six peaks, however, the effect is more profound in the main peak. As seen from Figure 5(e), the change of peak time takes place rapidly between 5.0 GHz and 10.0 GHz. A maximum delay in peak time of 72 s is observed among main peaks between high and low frequency ends. Such an unusual long delay may be attributed to the increase in the optical thickness of the microwave source at low frequencies (Takakura *et al.*, 1983). Please note that the delays for frequencies above turnover frequency (4–5 GHz) are more meaningful as they reflect emissions in the optically thin regime.

#### 4.2. ENERGY DEPENDENCE OF HARD X-RAY PEAK TIME

Similar comparisons of peak times are made for the X-ray data. The hard X-ray peak time  $t_p(E)$  is energy dependent. We illustrate this point by displaying a few X-ray total flux spectra obtained from the BATSE/LAD/DISCLA data. Only the first three available energy channels are useful. They are CH-1 (25–50 keV), CH-2 (50–100 keV), and CH-3 (100–300 keV).

The flux profiles for these channels are displayed in Figures 6(a–c). However, we are limited to work with the main peaks which are clearly identified in all three profiles. We observe a similar trend that as the energy of the channel increases, the hard X-ray peak appears earlier in time. The result is plotted in Figure 6(d). A difference in the peak time between CH-1 and CH-3 for the main peaks is found to be 10 s.

### 5. Conclusions

Hard X-rays and microwaves are generated by processes known as bremsstrahlung and gyro-synchrotron radiation respectively. The simple physical picture argues that electrons are trapped inside magnetic loops and they are responsible for emitting the two kinds of radiation. From the correlation study of derived observational parameters, we see that most of the time profile comparisons can be understood with existing physics.

As the hard X-ray flux increases, the microwave flux increases in all the frequencies; the microwave low-frequency index increases locally near the main peak (as indicated by the arrow in Figure 2(d)), which implies the inclusion of more non-thermal components; the hard X-ray power index decreases correspondingly, reflecting a harder electron distribution; the microwave peak flux increases, indicating larger emission measure in the emitting plasma; and finally the phase in the E-W baseline changes, signalling displacement of the source location. We find a rather low value for the low-frequency slope which is less than the minimum value of 2.0 for a thermal process. The discrepancy could be explained by the fact that the source size is a decreasing function of frequency.

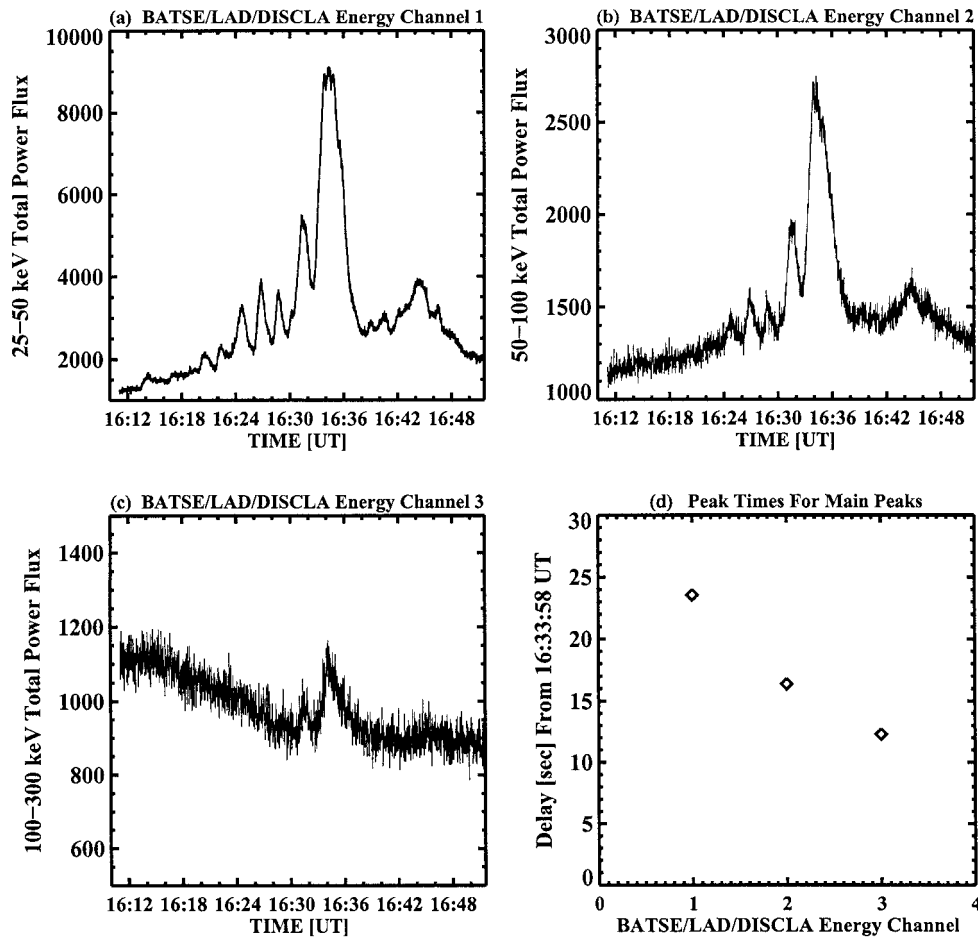


Figure 6. Three hard X-ray total flux profiles obtained from BATSE/LAD/DISCLA Detector 0 are shown in (a), (b), and (c). A plot of peak time versus channel number is given in (d) for the main peak. The peak time is observed to decrease as the channel number (energy) increases. A temporal resolution of one second is achieved, which is about twice as high as that of the 50 keV X-ray flux profile.

However, the fact that the temporal change of the microwave high-frequency spectral index does not follow that of the hard X-ray spectral index is not expected: they are out of phase with each other before, during and after the main peak. In the ‘trap-plus-precipitation’ model (Melrose and Brown, 1976; Aschwanden, 1998), energetic electrons with large pitch angles are trapped within a magnetic bottle and generate microwaves. If the distribution of pitch angles is not isotropic, we would expect a temporal increase in the capture of energetic electrons by the magnetic trap, while the fraction of free streaming electrons is momentarily reduced due to such perturbation. As a result, a temporal anti-correlation between the microwave optically thin index and the hard X-ray spectral index will be observed. The energy-

dependent loss by Coulomb collisions ( $dE/dt \sim -E^{-1/2}$ ) in the trap results in the accumulation of high energy electrons due to their longer lifetime. This fact is used to explain the hardening of non-thermal electron energy distribution (Melnikov and Magun, 1998). On the other hand, a double power-law energy spectrum for the energetic electrons has been investigated by Nitta *et al.* (1991) in order to explain the hardening of the power-law energy distribution index inferred from the microwave data with respect to the hard X-ray data.

A delay of the microwave peaks relative to the X-ray peaks is expected from previous observations and the electron trapping theory. This point is well illustrated by the plot of microwave peak flux versus hard X-ray photon counts. The 45 microwave flux profiles at different frequencies allow us to study the peak time as a function of frequency for each peak. It is observed that the peak time is frequency dependent and that the delay decreases as the frequency increases. A maximum delay of 72 s is found between the main peaks at different frequencies. It is an unusually long delay when compared with earlier results. On the other hand, we also notice that the peak time of the hard X-ray flux is energy dependent in the sense that hard X-ray flux at higher energies peaks earlier in time. However, a shorter delay of 10 s is found for the hard X-ray flux between different energies.

### Acknowledgements

We are grateful to Dr. D. Gary for reading the manuscript, and providing constructive criticism and OVRO data. We are also thankful to Dr. R. Schwartz for useful discussions, BATSE/LAD data, as well as software for data analysis. We also wish to thank the referee of this paper, Dr. S. M. White, for his helpful comments. This study is supported by NASA grant NAG5-3663.

### References

- Aschwanden, M. J.: 1998, *Astrophys. J.* **502**, 455.  
 Bastian, T. S. and Gary, D. E.: 1992, *Solar Phys.* **139**, 357.  
 Cornell, M. E., Hurford, G. J., Kiplinger, A. L., and Dennis, B. R.: 1984, *Astrophys. J.* **279**, 875.  
 Crannell, C. J., Frost, K. J., Matzler, C., Ohki, K., and Saba, J. L.: 1978, *Astrophys. J.* **223**, 620.  
 Dennis, B. R.: 1988, *Solar Phys.* **118**, 49.  
 Dennis, B. R. and Schwartz, R. A.: 1989, *Solar Phys.* **121**, 75.  
 Dulk, G. A.: 1985, *Ann. Rev. Astron. Astrophys.* **23**, 169.  
 Dulk, G. A., McLean, D. J., and Nelson, G. J.: 1985, in D. J. McLean and N. R. Labrum (eds.), *Solar Radiophysics*, Ch. 4, Cambridge University Press, Cambridge.  
 Gary, D. E., and Hurford, G. J.: 1989, in J. H. Waite, R. L. Burch, and R. L. Moore (eds), *Yosemite Conference on Outstanding Problems in Solar System Plasma Physics*, Geophysical Monograph 54, American Geophysical Union, Washington, DC, p. 237.  
 Gary, D. E. and Tang, F.: 1985, *Astrophys. J.* **288**, 385.  
 Kai, K., Nakajima, H., Kosugi, T., and Kane, S. R.: 1983, *Solar Phys.* **86**, 231.

- Kaufmann, P., Strauss, F. M., Costa, J. E. R., Dennis, B. R., Kiplinger, A., Frost, K. J., and Orwig, L. E.: 1983, *Solar Phys.* **84**, 311.
- Lu, E. T. and Petrosian, V.: 1990, *Astrophys. J.* **354**, 735.
- Marsh, K. A. and Hurford, G. J.: 1980, *Astrophys. J.* **240**, L111.
- Melnikov, V. F. and Magun, A.: 1998, *Solar Phys.* **178**, 153.
- Melrose, D. B. and Brown, J. C.: 1976, *Monthly Notices Royal Astron. Soc.* **176**, 15.
- Nitta, N., White, S. M., Schmahl, E. J., and Kundu, M. R.: 1991, *Solar Phys.* **132**, 125.
- Schwartz, R. A., Fishman, G., Meegan, C., Wilson, R., and Paciasas, W.: 1993, *Adv. Space Res.* **13**, 233.
- Silva, A. V. R., Wang, H., and Gary, D. E.: 1999, *Solar Phys.*, submitted.
- Stahli M., Gary, D. E., and Hurford, G. J.: 1989, *Solar Phys.* **120**, 351.
- Takakura, T., Degaonkar, S. S., Ohki, K., Kosugi, T., and Enome, S.: 1983, *Solar Phys.* **89**, 379.